Friction **7**(6): 637–650 (2019)
https://doi.org/10.1007/s40544-019-0259-5
ISSN 2223-7690
CN 10-1237/TH
RESEARCH ARTICLE

Interplay between microstructural evolution and tribo-chemistry during dry sliding of metals

Philipp G. GRÜTZMACHER[1,*], Sebastian RAMMACHER[1], Dominic RATHMANN[2], Christian MOTZ[2], Frank MÜCKLICH[1], Sebastian SUAREZ[1]

[1] *Chair of Functional Materials, Saarland University, Campus D3.3, Saarbrücken 66123, Germany*

[2] *Chair of Experimental Methodology of Material Science, Saarland University, Campus D2.2, Saarbrücken 66123, Germany*

Received: 26 July 2018 / Revised: 11 October 2018 / Accepted: 28 November 2018

Abstract: Understanding the microstructural and tribo-chemical processes during tribological loading is of utmost importance to further improve the tribological behavior of metals. In this study, the friction, wear and tribo-chemical behavior of Ni with different initial microstructures (nanocrystalline, bi-modal, coarse-grained) is investigated under dry sliding conditions. In particular, the interplay be-tween frictional response, microstructural evolution and tribo-oxidation is considered. Friction tests are carried out using ball-on-disk experiments with alumina balls as counter-bodies, varying the load between 1 and 5 N. The microstructural evolution as well as the chemical reactions beneath the samples' surface is investigated by means of cross-sections. The samples with finer microstructures show a faster run-in and lower maximum values of the coefficient of friction (COF) which can be attributed to higher oxidation kinetics and a higher hardness. It is observed that with increasing sliding cycles, a stable oxide layer is formed. Furthermore, initially coarse-grained samples show grain refinement, whereas initially finer microstructures undergo grain coarsening converging towards the same superficial grain size after 2,000 sliding cycles. Consequently, the experimental evidence supports that, irrespective of the initial microstructure, after a certain deformation almost identical steady-state COF values for all samples are achieved.

Keywords: dry sliding; microstructural analysis; tribo-oxidation; wear

1 Introduction

Even though the tribological analysis of pure metals is usually simplified by considering tribo-logical systems in which only a handful of parameters (load, velocity, total friction distance, etc.) are studied by a systematical variation, it is also evident that there are strong mutual influences between the material characteristics (e.g., surface finishing) and the resulting friction and wear behavior [1, 2]. Recently, the analysis has been extended by adding a materials science perspective, focusing particularly on the microstructural state of the friction surfaces. Besides the characteristic physical material properties (i.e., mechanical, thermal), different initial microstructures (from fine-grained to coarse-grained) are able to strongly influence the tribological properties [3, 4].

For example, previous reports have shown the possibility of significantly reducing friction in metals in the case of nanocrystalline compared to coarse-grained microstructures [3, 5]. These differences can be traced back to dissimilar wear mechanisms resulting from the different mechanical properties of the metals. Coarse-grained materials are softer than their fine-grained counterparts, hence favoring plastic deformation (mainly ploughing) as wear mechanism. As the real contact area tends to be enlarged by plastic deformation, this increases the coefficient of friction (COF) [6, 7].

* Corresponding author: Philipp G. GRÜTZMACHER, E-mail: philipp.gruetzmacher@uni-saarland.de

Additionally, the different wear mechanisms usually lead to higher wear rates for softer, coarse-grained materials compared to fine-grained materials [6, 7]. Finally, the tribo-oxidation of the contact is also influenced by the initial microstructure [8]. In this context, it has been shown by Shafiei and Alpas that the grain boundaries serve as preferred nucleation sites for oxides and that diffusion along the grain boundaries is enhanced [6]. Therefore, oxidation is faster for finer microstructures [6]. Once these oxides are formed they can be mechanically mixed with pure metal to form a nanocomposite under sliding [9].

Another important factor is the microstructural evolution of the metal as a result of the intermittent tribological loading. Several publications (e.g., Rigney et al., Prasad et al., or Qi et al.) report in the case of an initially coarse-grained microstructure on the formation of a narrow layer of several 10 nm in depth where a significant grain refinement could be observed [10–12]. This layer is consistently reported to be located right in the immediate sub-surface of the wear scar. The authors consider this nanocrystalline tribologically-induced layer to be responsible for the wear rate stabilization and the reduction of friction (reduction of real contact area) due to its increased hardness. Furthermore, Cordill et al. observed a microstructural fragmentation in the tribologically-influenced zone below the wear scar of Ni single crystals [13]. The formation mechanism of the layer is still not clear, but there are strong indications of a mechanism based on the movement and rearrangement of dislocations [13].

In contrast to the grain refinement for coarse-grained materials, several reports observed a slow grain coarsening of initially nanocrystalline materials during tribological loading [4, 11, 14, 15]. Considering both, tribologically induced refinement and coarsening, Argibay et al. postulate the existence of an equilibrium grain size for a specific set of initial grain size and tribological stressing condition [4]. Similar considerations can be found in corresponding publications for the microstructural changes in metals subjected to severe plastic deformation (SPD) techniques such as ball milling or high pressure torsion (HPT) [16–20].

It is thus evident that microstructural changes induced by tribological loading are indeed related to the initial microstructure (especially grain size) and the tribological stressing condition. The microstructural state of the material, in turn, influences the friction and wear behavior of the rubbing surfaces. To further investigate and rationalize these dependencies, pure Ni with three different initial microstructures was tribologically tested in this study with different load levels. In addition to a comparative COF analysis, the tribologically-induced microstructural changes were analyzed as a function of the initial microstructure, load and sliding cycle number, by means of cross sections at each wear scar center. This analysis enables a deeper understanding of the evolution of the microstructural changes and their link to the corresponding friction and wear behavior.

2 Experimental procedure

2.1 Material

Pure nickel with three different initial mean grain sizes and microstructures was selected because of its single-phase microstructure to study the effect of tribological loading on the initial microstructure and vice-versa. Ni is a model material, which has been extensively tested for the understanding of microstructural processes.

Representing a sample with a small initial grain size, nanocrystalline (nc) nickel samples were manufactured by electrochemical deposition onto a copper cathode. The exact composition of the electrochemical bath and the deposition parameters can be seen from Table 1.

Furthermore, samples with a bimodal microstructure were produced by heat-treating the aforementioned nc samples at 210 °C for 150 minutes. Finally, coarse-grained (cg) nickel samples were manufactured by a powder metallurgical process. This process involves

Table 1 Composition of the electrochemical bath and deposition parameters for the electrochemical deposition of nanocrystalline nickel.

Parameter	Value
Nickel sulfamate（mL/L)	595
Nickel chloride hexahydrate (g/L)	5
Boric acid (g/L)	35
Sodium lauryl sulfate (g/L)	0.2
Saccharin sodium (g/L)	0.4
pH value of the bath	3.5−3.7
Bath temperature (°C)	45

cold pressing of dendritic nickel powder (mesh-325, Alfa Aesar, Germany) and subsequent sintering by hot uniaxial pressing (HUP) at 750 °C and 264 MPa under vacuum conditions (2×10^{-4} Pa) for 150 min. As a result, coarse-grained nickel samples with a typical residual porosity of <4% are obtained.

For the nc samples, X-ray diffraction was used to calculate the grain size by analyzing the diffraction peak broadening which is related to the grain size. Therefore, an X-ray diffractogram from 2θ = 35° to 125° was recorded and the mean grain size ($D_{\text{mean, nc}}$ = 40 nm) was calculated by means of the Williamson-Hall method [21].

For the bimodal samples it can be assumed that during heat treatment only part of the nc grains show significant grain growth, whereas the rest of the grains remain in their initial state. The mean grain size of the grown grains was determined by electron backscatter diffraction (EBSD). As a result of this analysis the samples can be described with a bimodal microstructure with nc grains ($D_{\text{mean, nc}}$ = 40 nm) and ultra-fine grains (ufg) ($D_{\text{mean, ufg}}$ = 650 ± 240 nm).

The mean grain size of the coarse-grained, sintered samples was also determined by EBSD and amounts to $D_{\text{mean, cg}}$ = 6.58 ± 5.29 μm. Figure 1 shows a schematic representation of the three different microstructures and sample types.

The sample's hardness, which varies due to their different initial grain size, is determined with a microindenter (DuraScan G5, Struers) using the Vickers method (HV0.025 = 0.245 N). Table 2 shows the results in GPa of 25 indents for each sample as well as the counterpart's hardness as specified by the supplier.

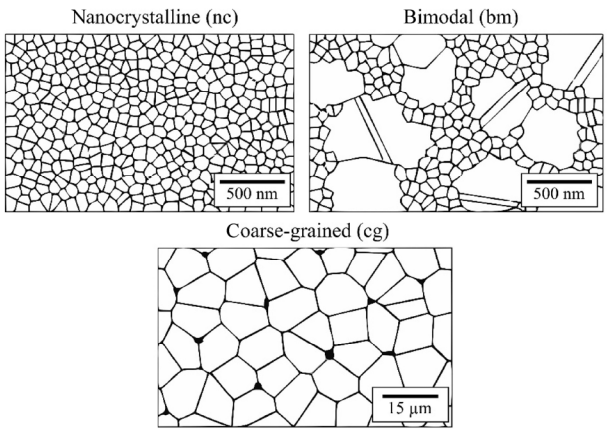

Fig. 1 Schematic representation of the three different evaluated microstructures.

Table 2 Hardness values of the evaluated microstructures.

Sample	Hardness (GPa)
Nanocrystalline (nc)	5.8 ± 0.3
Bimodal (bm)	4.7 ± 0.2
Coarse-grained (cg)	1.2 ± 0.04
Al_2O_3 counterpart	17.7

2.2 Surface analysis and contact characteristics

All samples were ground and polished with a polishing machine (Tegra Force 5, Struers). Subsequently finer grinding steps (320–2,500) were used. Finally, the samples were polished with various diamond suspensions (6 μm, 3 μm, 1 μm) and an oxide polishing suspension (OPS) to obtain their final roughness. The roughness parameters S_q, S_k and S_{pk} of the nickel samples as well as the tribological counterpart (alumina ball) were measured by means of a confocal laser scanning microscope (CLSM) (OLS 4000, Olympus) prior to the tribological tests. S_q is the RMS roughness (root mean square mean of the profile heights), S_k is the core roughness (core height of the profile along the depth, used to evaluate the load-bearing capacity) and S_{pk} indicates the peak height of the asperities. Table 3 shows the results of these measurements. The cg samples show slightly increased roughness values due to their residual porosity.

The surface parameters obtained by microscopy analysis were also used to estimate the contact pressures acting between the tribological pairs in the case of static loading. The pressures were calculated taking the Hertzian model as a basis [22]. The resulting contact pressures at the center of the contact area are 1.91, 2.41 and 3.26 GPa for 1, 2 and 5 N, respectively.

For the determination of the contact radius, it is assumed that the contact is of elastic nature (Hertzian contact) between nominally flat surfaces. Hence, the contact radius a can be estimated by [23]:

Table 3 Surface descriptive parameters of the evaluated microstructures and tribological counterpart.

Sample	S_q (nm)	S_k (nm)	S_{pk} (nm)
Nanocrystalline (nc)	2.1 ± 0.4	5.4 ± 1.0	2.4 ± 1.0
Bimodal (bm)	3.3 ± 1.0	7.5 ± 1.0	4.3 ± 1.0
Coarse-grained (cg)	10.8 ± 2.0	15.5 ± 2.0	11.7 ± 3.0
Al_2O_3 counterpart	0.3 ± 0.2	—	—

$$a = \sqrt[3]{\frac{3 \cdot F}{8} \cdot \frac{((1-\nu_1^2)/E_1)+((1-\nu_2^2)/E_2)}{1/d_1+1/d_2}} \quad (1)$$

where F is the load, υ is the Poisson coefficient, E is the elastic modulus, and d is the diameter of the sphere. The subscript denotes the two contacting bodies. Under this assumption, the contact radius for the different experimental loads is 25.4, 32.0 and 43.4 μm for 1, 2 and 5 N, respectively.

Additionally, scanning electron microscopy (SEM) (Helios Nanolab 600, FEI) is used after tribological testing to observe the appearance of wear scars and debris at high magnification and thus determine the prevailing wear mechanisms.

2.3 Tribological characterization

The tribological experiments were conducted by means of a ball-on-disc micro-tribometer (*CSM Instruments*) in bi-directional linear-reciprocating sliding mode (a full cycle is defined as a complete round trip of the counterpart). The tribometer was placed within an environmental chamber to control temperature and humidity during the experiments. Alumina (Al_2O_3) balls with a diameter of 1.5 mm served as counter body (Anton Paar GmbH, Germany). Various normal forces were used to study the effect of increasing load on the frictional properties as a function of the samples' microstructures. The experiments were stopped after 5, 50, 500 and 5,000 cycles to study the evolution of the microstructure during the frictional testing. Regarding the evaluation of the acquired data, a trimming of the full COF cycle by removing the ends of the curve was performed, thereby focusing only on the dynamic part of the COF.

Each experiment was repeated five times. The environmental and experimental settings are shown in Table 4.

Table 4 Parameters of the tribological experiments.

Parameter	Unit	Value
Temperature T	°C	25
Relative humidity H_{rel}	%	35
Load F_N	N	1, 2, 5
Sliding velocity v	mm/s	5
Stroke length Δ	mm	2.3

An important characteristic of non-lubricated sliding is the interfacial temperature increase within the contact region. Based on the simplified model described by Hutchings et al., the rate of heat generation per unit area at the contact region relates the dissipated frictional heat through the contact area [24]:

$$q = \frac{\mu \cdot F_N \cdot v}{\pi \cdot a^2} = \frac{\text{dissipated frictional power}}{\text{contact area}} \quad (2)$$

where μ is the coefficient of friction, F_N is the normal load, v is the sliding velocity, and a is the Hertzian contact radius. From this value, it is possible to determine the local increment in temperature at the contact region, usually known as flash temperature (ΔT_f), with the following equation:

$$\Delta T_f = \frac{q \cdot a}{\lambda} \quad (3)$$

Considering that the thermal conductivity of nickel and alumina is λ_{Ni} = 90.7 W/(m·K) and $\lambda_{Al_2O_3}$ = 35 W/(m·K), respectively, the temperature rise in the contact region is marginal, as shown in Table 5 [25].

These low values are a consequence of the low testing speed, which allows the generated frictional heat to be effectively removed throughout the experiment.

2.4 Chemical and microstructural characterization

The initial and final chemical composition of the surfaces was evaluated using energy dispersive X-ray spectroscopy (EDS) in a SEM. Regarding the initial composition, especially the presence of impurities or oxygen layers after the polishing process is analyzed since these can significantly alter the tribological behavior. After tribological testing, EDS was used to analyze tribochemical reaction layers.

Microstructural changes as a result of the tribological loading were analyzed by preparing cross-sections of the wear scars. Therefore, in a first step the samples' surface is protected by an electrochemically deposited,

Table 5 Temperature rise values for the experimental loads.

F_N (N)	q (MW·m^{-2})	ΔT_f (Ni) (K)	ΔT_f (Al_2O_3) (K)
1	0.743	0.21	0.54
2	0.936	0.33	0.85
5	1.270	0.61	1.57

nanocrystalline Ni layer which is capable to prevent preparation artifacts during the metallographic processing. Afterwards, the samples are cut at the region of interest (ROI) with a diamond wire saw and the cross-sections are polished by an additional metallographic preparation (same as described in Section 2.2), so as to completely remove the region affected by the cutting. In this study, the selected ROI is the middle of the wear scar in both directions (perpendicular and parallel to the sliding direction). At this position the stability of the tribometer movement as well as the sliding velocity and thus shear stress on the surface are at their maximum. Hence, the maximum microstructural changes due to the tribological loading can be expected there.

The cross-sections were evaluated for each initial grain size, load as well as after 5, 50, 500 and 5,000 cycles. SEM and EBSD were used to analyze the stress and cycle dependent microstructural changes in the influenced zones, e.g., grain size and depth of the substructures. The chemical composition of the substructures and tribochemical layers were determined by means of EDS. TEM analysis was performed using a JEOL JEM 2010F at an acceleration voltage of 200 kV.

3 Results and discussion

3.1 Stress and cycle dependent tribological behavior

3.1.1 Friction analysis

In order to investigate the effect of the initial microstructure on the frictional behavior during run-in, low-cycle experiments have been performed. In Fig. 2, the COF of the three different microstructures (nc, bm, cg) is plotted against the cycle number. As can be seen, all samples, independent of initial microstructure and load, start at a similar COF of about 0.2. Furthermore, regardless of the experimental parameters, a similar evolution of the friction coefficient over time can be observed, with the COF first increasing to its maximum (μ_{peak}) and then decreasing again until a steady COF is reached (μ_{steady}). This curve shape is typical for the run-in of metallic materials under dry friction and has already been discussed by Blau [26]. During the first cycles the highest asperities are worn off, leading to an increase of the real contact area and thus to a higher COF. The increased COF at μ_{peak} is also related to the plastic deformation of the bulk material at high contact pressures.

As can be further seen from Fig. 2, the differences in frictional behavior are only apparent during the first 20 to 30 cycles of run-in. The only case in which a noticeable difference in COF over the entire measuring time is observed is in the cg sample at 1 N (Fig. 2(a)). This can be attributed to an increased real contact area due to high plastic deformation and material pile-up at the sides of the wear track, when compared within the same experimental load to the other two considered microstructures.

Additionally, a dependence between the cycle number after which μ_{peak} and μ_{steady} are reached and the initial microstructure is observed. The peak value of the nc material is reached after only 4 to 5 cycles, whereas the bimodal sample reaches its' maximum COF value after 7 to 8 cycles and the cg material even after 10 to 12. Moreover, the nc sample is also the first to reach steady state friction (μ_{steady}). The faster run-in can be traced back to a quicker oxidation of the nc samples and a faster stabilization of the wear track as well as the microstructure. Since finer microstructures possess a larger amount of grain boundaries (that act as oxygen diffusion paths), their oxidation kinetics differ from their coarser counterparts, rendering them more prone to oxidation [6]. Another factor playing a role in the faster run-in behavior of the nc microstructure might be that an inverse Hall Petch behavior

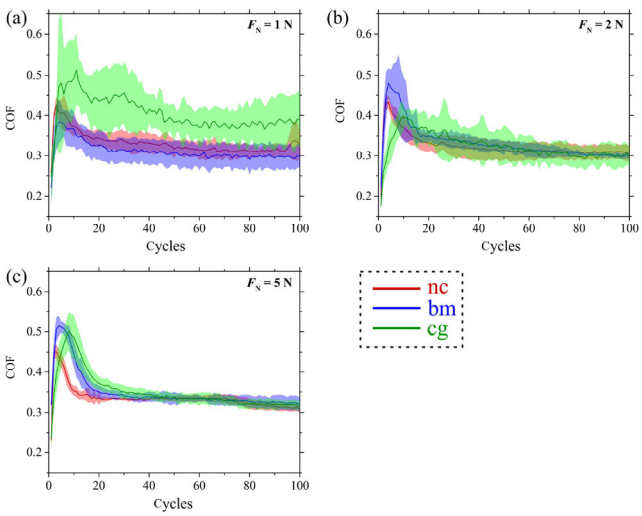

Fig. 2 Short-term evolution of the coefficient of friction (COF) tested at (a) 1 N, (b) 2 N, and (c) 5 N of normal load. The shaded areas represent the standard deviation of the tests.

is involved, favoring grain boundary sliding and reducing the interfacial shear strength, leading to an easier intermixing between a superficial oxide layer and the bare metal [27]. The generation of brittle interfaces (as a consequence of GB oxidation) leads to a process, similar to what happens at the Hall-Petch breakdown region (grain boundary sliding) that may stabilize the real contact area.

The peak value μ_{peak} is load dependent whereby it increases with increasing normal load. Again, the cg material is an exception to this, since it shows a smaller μ_{peak} for the load of 2 N compared to 1 N. The load-dependent COF can be explained by a greater plastic deformation due to higher contact pressures for higher loads, which leads to a higher real contact area. Thereby, the nc material generally shows lower peak values compared to the other microstructures, which can be attributed to the differences in hardness. Being in contact with the hard counter body, the softer metallic samples are subjected to plastic deformation. If the substrate is less hard, a more pronounced deformation (higher penetration of the counter body) is to be expected. This results in a larger real contact area for the softer materials and thus higher peak values μ_{peak}. The relationship between the hardness of the material and the peak value of the COF has already been observed and discussed by Shafiei and Alpas [6]. Moreover, plastic deformation as a wear mechanism is reasonable when analyzing the wear track topographies (see Section 3.1.3). In order to verify that after 100 cycles steady state conditions are reached, high-cycle experiments were performed. Figure 3 shows the COF of all tested microstructures for 5 N over 5,000 sliding cycles. It can be seen that run-in is completed after 1,000 cycles at most. After this short running-in period there is virtually no difference in COF between the different samples. Hence, the steady state value is the same for all tested samples ($\mu_{steady} \approx 0.3$) with respect to the given standard deviations and independent of load or initial microstructure.

3.1.2 *Tribo-oxidation*

The previously described frictional behavior can be associated with the formation of a thermodynamically stable oxide layer as well as to a strengthening effect

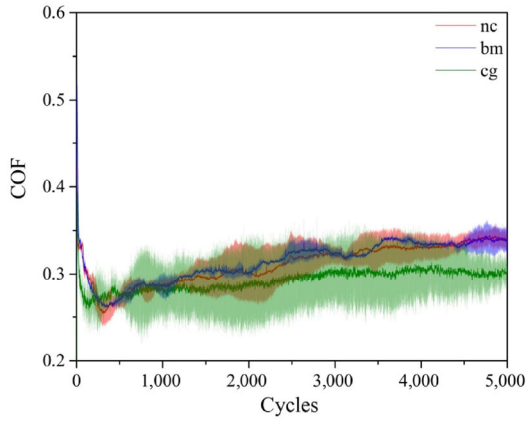

Fig. 3 High-cycle evolution of the COF (up to 5,000 sliding cycles) of all tested microstructures at a normal load of 5 N. The shaded areas represent the standard deviation of the tests.

induced by microstructural modifications. Regarding the contact conditions, especially, the oxide layer which is formed during tribological testing (transition from plasticity-dominated towards oxidative wear) creates comparable conditions between substrate and counter body for all tested microstructures and thus leads to similar steady state COF values. The oxidation of the wear track can be clearly seen in Fig. 4, which exemplarily shows the EDS maps of the nc sample after 10 cycles at 1 N. Shortly before reaching steady state, the oxide layer is not yet completely covering the surface. The distribution of oxygen within the measured area indicates that even at a low cycle number, there is spallation of the oxide layer. Moreover, the electron micrograph in Fig. 4(a) shows early signs of galling of the metal.

Additional EDS line scans in Fig. 5 along the cross-section (here after 5000 sliding cycles) further prove the existence of oxide at the sample immediate sub-surface. Interestingly, all samples show a comparable O-containing region of approximately 2 μm in depth. This is unexpected, since it is usually observed that the oxidation is stronger in finer microstructures as a result of a larger amount of grain boundaries, which act as diffusion paths. Nevertheless, due to said reasons oxidation is faster for the finer microstructures. It is worth mentioning that a quantification of the partial concentrations of O and Ni is, for the available characterization equipment, not reliable and hence is left out of the discussion in the manuscript.

Up to 5,000 sliding cycles the oxide layer might be generated, broken, integrated to the uppermost layer

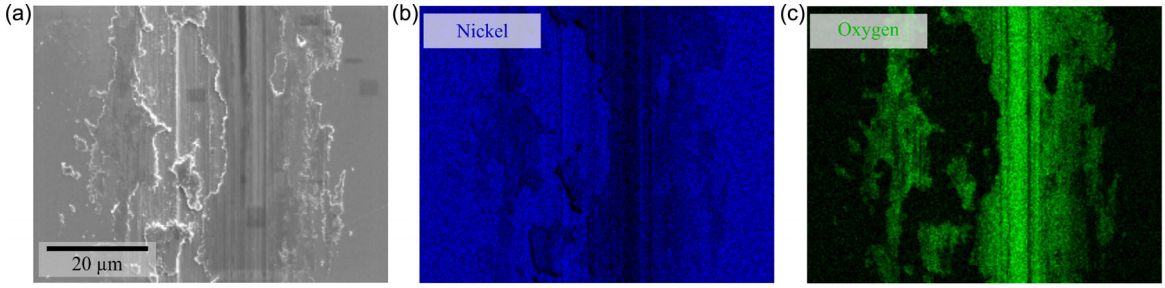

Fig. 4 Wear track after 10 sliding cycles at 1 N of the nc sample. (a) High resolution electron micrograph for (b) corresponding Ni and (c) oxygen EDS concentration maps.

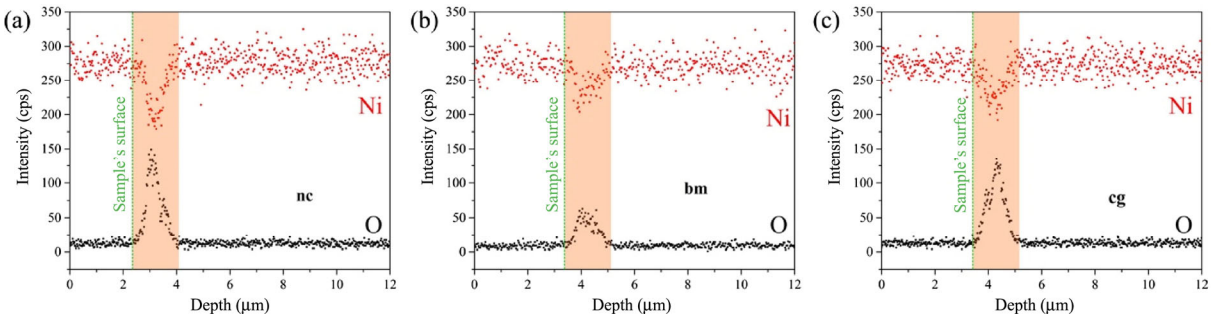

Fig. 5 Chemical concentration profile (EDS line scan) along the cross-section of (a) the coarse-grained, (b) the nanocrystalline, and (c) bimodal sample after 5,000 sliding cycles measured with a normal force of 5 N.

and regenerated (in the bare metal regions) whereby at some positions a thickness of 2 μm can be observed [9]. This value lays within the critical oxide thickness value (ξ_c) reported for metals by Sullivan et al., which represents the critical size at which the oxide film becomes mechanically unstable and is removed, favoring its incorporation to the wear process [28]. Additionally, it has been shown that the oxidation kinetics of metals under sliding conditions can be up to several orders of magnitude faster (especially at low temperatures) than that of static (thermal) oxidation [28]. The higher oxidation kinetics of metals subjected to dry sliding is given by the high content of lattice defects as a consequence of the mechanical perturbation. This perturbation may also lead to a recrystallization process in the metal. It is known that an important factor for oxidation is the total length of grain boundaries which provide enhanced oxygen diffusion paths that favor the intergranular oxidation of the metal, resulting in brittle interfaces [6]. Consequently, tribo-oxidation and thus running-in of the cg samples is slightly delayed compared to the samples with a small initial grain size. Furthermore, the brittle oxide interfaces tend to break and are subsequently intermixed with the native metal forming a metal/oxide composite (see Section 3.2).

3.1.3 *Wear analysis*

Figure 6 shows the wear track morphologies of the three different samples types. For the softer materials (cg, bm), material pile-up can be noticed at the wear track edges after 5 sliding cycles. The morphology of the nc samples' wear track varies essentially from the bm and cg samples. There is far less material pile-up and the wear track width is reduced significantly. Thereby, it is interesting to note that the wear track depth of the nc and cg sample is almost identical. The differences in wear track morphology are a result of different wear mechanisms which is also reflected when analyzing the proportions of microploughing and microcutting according to Zum Gahr [29]. The former mechanism consists of the plastic deformation and pile-up of the material during contact, whereas in the latter, all the tribologically influenced volume is completely removed from the wear scar as third bodies. Table 6 shows the cutting efficiency (f_{ab}) values after 5 sliding cycles. Since higher values correspond to microcutting as the main wear mechanism (corresponds

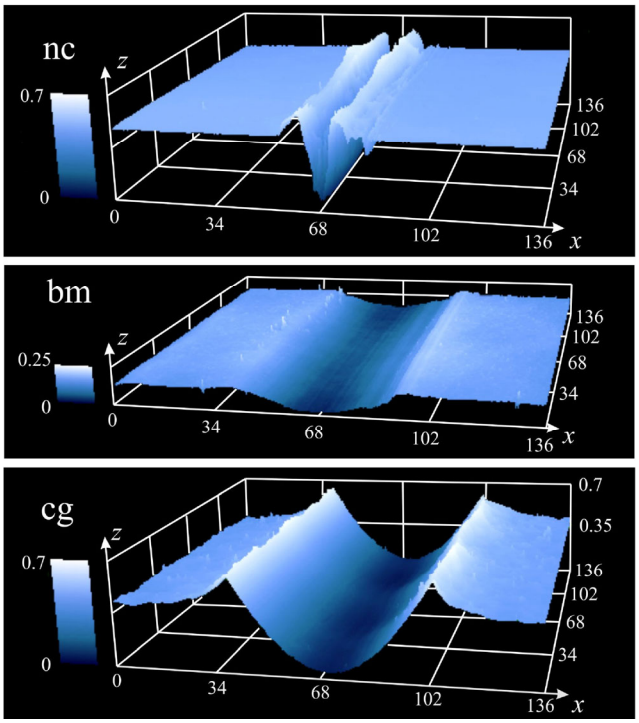

Fig. 6 Wear track profiles for all samples tested with a load of 5 N after 5 sliding cycles. Note that the values are in µm.

Table 6 Cutting efficiency values (f_{ab}) obtained from the wear track profiles for the tested samples.

Sample	f_{ab}
Nanocrystalline (nc)	0.8 ± 0.1
Bimodal (bm)	0.5 ± 0.1
Coarse-grained (cg)	0.2 ± 0.1

to f_{ab} = 1), it can be concluded that the nc samples show predominantly microcutting, whereas the cg samples show a stronger trend towards micro-ploughing (corresponds to f_{ab} = 0), and the bm samples lie in between. The observed differences can be associated with a higher ductility of the samples comprising larger grains. Thereby, the ductility of the respective samples is inversely proportional to their hardness. The behavior of the bm sample can be explained by their partially coarser grains. These grains provide sufficient ductility to avoid complete microcutting. On the other hand, even the coarser grains are much smaller than in the cg case which is why the bm sample shows a less ductile behavior. Additionally, due to the faster oxidation and thus rather brittle behavior of the nc samples, the occurrence of third bodies is far more likely leading to abrasive wear between the substrate and third body particles.

Over time, there is a transition from plasticity-dominated to oxidative wear, which has been demonstrated in Section 3.1.2 by the EDS investigations. Due to the generation of the hard and brittle nickel oxide for all samples, the wear track topographies as well as the dominating wear mechanism are equalized.

3.2 Cycle-dependent microstructural development

In order to further interpret and discuss the experimental findings shown in the previous section, the microstructural evolution during the tribological experiment was investigated based on cross-sections through the wear track. The focus of the analysis is shifted towards the samples stressed with the higher load (5 N), where the effects are markedly noticeable. The aforementioned cross-sections were prepared after 5, 50, 500 and 5,000 sliding cycles.

Figures 7(a)–7(d) shows the microstructural evolution of the nc samples. It is worth mentioning that all normal loads show a similar evolution of the microstructure, which is why the depicted images are representative for all tested normal loads. On top of the wear track (upper part of the images), a protective layer of electrochemically deposited nanocrystalline Ni can be seen (highlighted in red in the image).

After only 5 sliding cycles (Fig. 7(a)) a change in microstructure close to the surface of the wear track can be noticed. Directly underneath the wear track up to a depth of 200 nm, some slightly larger grains can be detected. Following this topmost layer, a zone with noticeable grain coarsening develops. The largest grains have a grain size D_{max} of 270 nm and are therefore considerably larger than the initial grain size of 40 nm.

As identified by Hutchings and Shipway for dry sliding wear, three main different regions can be observed (shown schematically in Fig. 8), namely [24]:

- Zone 1: composite region consisting of a mixture of the base metal and oxide particles.
- Zone 2: region of plastic deformation, which, depending on the initial microstructure, would show either grain refinement or coarsening.
- Zone 3: the lowermost, unaffected region showing the original microstructure.

The Zones 1 and 2 are what is usually named as the *Tribologically Transformed Zone* (TTZ). Below this zone,

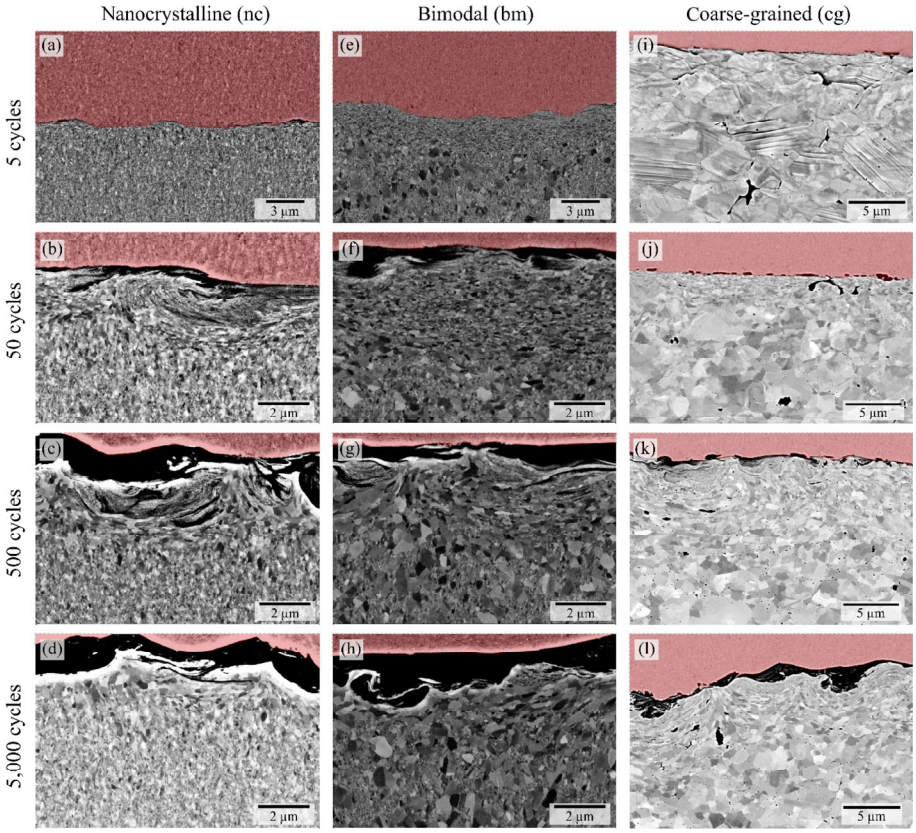

Fig. 7 Microstructural evolution for the tested microstructures after: 5, 50, 500 and 5,000 cycles and normal loading of 5 N. The red shaded regions mark the protective Ni coating.

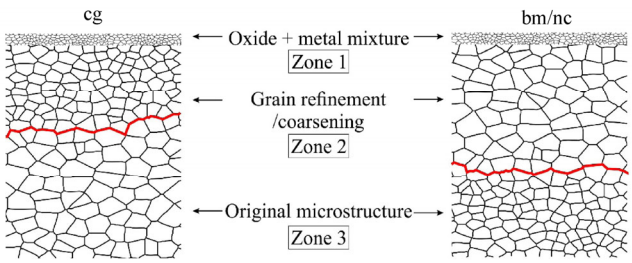

Fig. 8 Schematic representation of the usually observed microstructural regions in dry sliding. The microstructures are represented with an arbitrary scale.

in the case of the nc samples at a depth of roughly 1 μm or higher, the microstructure stays unaffected and shows the initial condition. Up to 500 sliding cycles the thickness of the TTZ rapidly increases to roughly 4 μm whereas after this, it only marginally increases. After 5,000 sliding cycles, the D_{max} in Zone 2 has increased to 680 nm.

The microstructural development of the bm samples is similar to the one already observed for the nc samples (Figs. 7(e)–7(h)). As can be seen, there is also a layer of nanocrystalline grains followed by a transition zone with coarser grains. With increasing depth, the microstructure transitions into the primary microstructure until the initial grain size is reached. After 5 cycles, the maximum depth of the TTZ in which a change in microstructure can be detected is slightly larger (roughly 2 μm) than that of the nc samples at all measuring points. Thereby, the maximum grain size D_{max} in Zone 2 is roughly 700 nm, which is almost identical to D_{max} for the nc samples. The wider influenced zone for the bm samples is related to a lower initial overall hardness of the bm microstructure. It is worth mentioning that inside the TTZ, the bimodal microstructure is not recognizable anymore and, after merely 5 sliding cycles, a monomodal grain size distribution is observed.

Regarding the cg samples (Figs. 7(i)–7(l)), their microstructural evolution is rather different compared to that of the nc and bm samples. In contrast to the samples with a smaller initial grain size, the cg sample does not show grain coarsening but grain refinement.

The depth of the TTZ exceeds 10 μm and is thus, much larger than that of the nc and bm samples. It can be concluded that the depth of the influenced zone is increasing with decreasing initial hardness of the substrate material. The initial microstructure with a mean grain size of 6.58 μm is only vaguely recognizable. Inside the initial grains, much smaller subgrains can be found. The generation of these subgrains follows a defined sequence of several steps, which end in the fragmentation of the original microstructure. During the stressing of the metal in the plastic regime, geometrically necessary dislocations (GND) are generated to accommodate deformations, partitioning the original grains and arranging themselves into dislocation sub-cells. These cells are subsequently rotated (as a consequence of the plastic strain), thus forming low-angle grain boundaries. With accumulated strain, a stabilization towards high-angle grain boundaries is achievable, thus reaching a steady state. Similar processes are happening during SPD and are well documented in the literature [19, 30]. For example, Pippan et al. observed a sharp increase in the high-angle boundary fraction of a Ni single crystal at an equivalent strain of 5 in torsionally-deformed Ni [19]. The ongoing high plastic deformation during tribological testing could similarly lead to a fragmentation of the initial grains into sub-grains. Another aspect which leads to the fragmentation of the initial grains is the formation of geometrically necessary boundaries (GNBs) which is known to occur in deformed polycrystalline microstructures. These GNBs accommodate the lattice misorientations, which result from dislocation gliding on the different slip systems and usually are formed in a parallel manner [31]. An example is shown in Fig. 9, which illustrates this process. The initial grain boundaries are still visible and some of them are highlighted by green lines. Within the original grains, the smaller generated subdomains are clearly noticeable (highlighted in blue). Additionally, Rigney et al. and Heilmann et al. made similar observations during the tribological testing of cg metallic materials [32, 33].

The minimum grain size of the generated subgrains is between 100 nm and 200 nm, which accounts for a strong decrease compared to the initial grain size of 6.58 μm. The smallest grains can be found close to the surface and with increasing distance from the surface the grain size is increasing until the original microstructure can be observed again. The maximum grain size close to the frictional contact area D_{max} for the cg samples is roughly 1,000 nm after 5,000 sliding cycles (Fig. 10), which is within the same range as for the other two sample sets (nc, bm) with smaller initial grain sizes.

For all sample types a continuous oxide layer can be detected on top of the wear track which is in accordance with the previously shown EDS investigation. Monotonically increased shear strain leads to the rupture of the tribologically-induced oxide layer and the mechanical intermixing of the generated third bodies and the soft metal [24]. This transition from a single-phase to a dual-phase material (composite-type Ni/NiO) acts on the dynamic recrystallization and

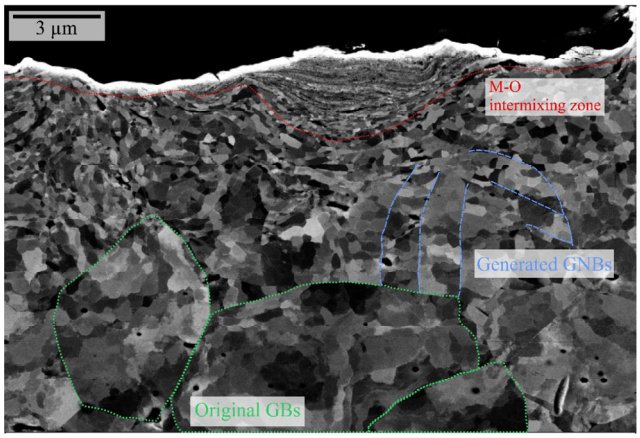

Fig. 9 BSE image showing the development of sub-grains inside the initial grains of the coarse-grained sample after 5,000 sliding cycles at 5 N.

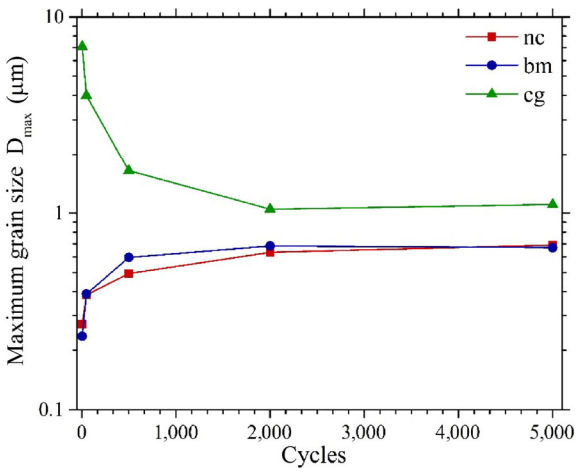

Fig. 10 Evolution of the maximum grain size D_{max} over the cycle number for all three initial microstructures at 5 N.

helps in the microstructural stabilization (saturation of grain size) by pinning of grain boundaries and a delay in the microstructural recovery due to hindering of dislocation mobility [34]. This renders very small grains within the composite zones of nickel oxide and pure nickel. The composite zone creates similar contact conditions and thus is one of the factors responsible for stabilizing and equalizing the COF. In general, the oxide formation for the bm and cg samples seems to be a little slower since less oxide can be detected after 500 sliding cycles. This can be assumed as a possible explanation for a slower running-in process and adjustment of steady-state conditions compared to the nc samples, especially at 5 N (see Fig. 2).

Furthermore, wavy structures can be observed for higher sliding cycles inside the composite zones. The swirled morphology of the uppermost layer in all cases could be related to the contact shear stress distribution throughout the depth of the contact region. Considering that the shear stress reaches its maximum below the surface (at a depth of approximately half the contact radius a) and the surface shear stress is non-zero (Fig. 11), the resulting shear force unbalance leads to a relative circular motion of the plastic flow, aiding the mechanical intermixing between the metal and the broken oxide scale [23]. Within Zone 1, it is not possible to unequivocally identify any grains and the oxide is finely mixed with nickel.

Considering the values previously determined in the experimental section based on the mentioned Hertzian contact model, the depth at which the shear stress (force) reaches its maximum would be 12.7, 16.0, and 21.7 μm. This results in the development of wave-like segments below the wear track at higher cycle numbers (see for example Figs. 7(b) and 7(c)).

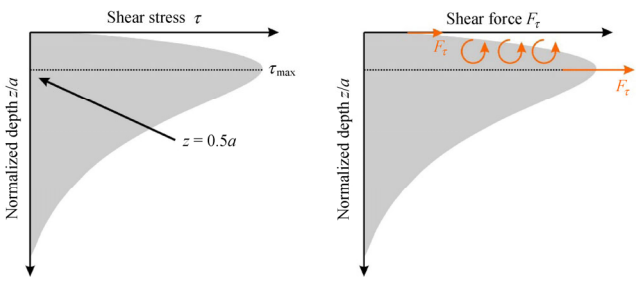

Fig. 11 Distribution of the shear stress and shear force throughout the depth of the contact region. The maximum value is located at a depth of approximately half of the Hertzian contact radius a.

At higher sliding cycles, a grain elongation perpendicular to the sliding direction can be noticed (Fig. 7(d)). Similar effects have been observed during severe plastic deformation of metals by high pressure torsion (HPT) [19]. Pippan et al. demonstrate a grain elongation for low temperatures (at which diffusion processes are usually restricted), generated by stress-induced grain boundary movement. They conclude that the deformation process occurs by sliding along the microstructural boundaries. At higher temperatures however, the grains become continuously more equiaxed [19]. It can be assumed that similar processes may occur in the TTZ, which indicates that the microstructural evolution could be stress-induced and not thermally driven (in agreement with the calculations of the flash temperature). To further examine if an elongation of the grains in the sliding direction is also noticeable, TEM foils were prepared parallel to the sliding direction (as shown in Fig. 12). In agreement with the cross-sections, the TEM measurement in Fig. 12 shows, using the bm sample as an example, the oxide layer and a zone with coarser grains. The elongation of the grains close to the surface parallel to the sliding direction is also clearly visible. This elongation results from large shear stresses close to the surface generated by the tangential force during friction.

In summary, all samples show a fast growth of a continuous oxide layer whereby the number of sliding cycles until this oxide layer is covering the entire

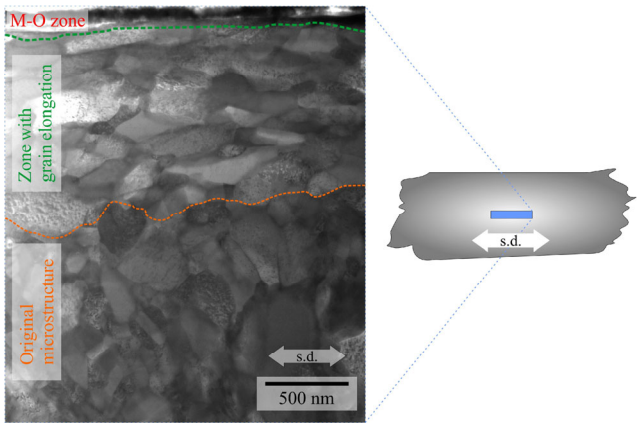

Fig. 12 Transmission electron micrograph of the sub-surface of the bm sample after 5,000 cycles under a 5 N load. The TEM foil was taken along the sliding axis at the center of the wear track, as shown in the schema on the right.

surface depends on the initial microstructure. The fastest growth can be observed for the nc sample and the slowest for the cg sample due to the increased total length of the grain boundaries, as discussed earlier. Subsequently, this oxide layer is fractured and intermixed with the soft metal. The superficial composite of oxide and metal causes similar contact conditions irrespective of the microstructure underneath. Furthermore, the composite slows down microstructural and topographical changes and thus steady-state condition settles in. After at most 500 sliding cycles (depending on the initial microstructure), there is oxide-oxide contact which leads to smaller and stable COFs. The depth of the influenced zone is increasing strongly during the first 500 sliding cycles for all microstructures and afterwards only slightly increases. Thereby, the depth of the TTZ is highly dependent on the initial microstructure and consequently on the hardness. It could be shown that a smaller initial microstructure and thus higher hardness leads to a less extended zone in which the microstructure has been influenced.

However, close to the tribologically loaded contact area the maximum grain size D_{max} for all samples is approaching a similar value between 680 nm and 1,000 nm with increasing cycle number as shown in Fig. 10. Thereby, the cg sample undergoes grain refinement whereas the grain size is coarsened for the nc/bm microstructure, converging towards a "stable" grain size. The former is generated by the continuous generation of GNDs, whereas the latter is driven by grain boundary mobility as a consequence of strain energy minimization [35]. This relationship between grain-coarsening for small initial microstructures and grain refinement for coarse initial microstructures has also been found during SPD and exemplifies the analogies of both processes [19]. As reported by Pippan et al. [19], if saturation during deformation of a single-phase material is reached, the resulting microstructure always ends up within the same equilibrium size range, independently of the initial state (i.e., independently of whether the initial structure was coarse- or fine-grained).

Taking the evolution of the maximum grain size (Fig. 10) together with the formation of a continuous oxide layer on top of the wear track into consideration, it is not surprising that the frictional response of all initial microstructures is similar after only few sliding cycles.

4 Conclusions

The frictional, wear and tribochemical behavior of Ni with different initial grain sizes was investigated under dry sliding conditions. The friction tests were conducted on a ball-on-disk setup in linear-reciprocating sliding mode with alumina balls as counter bodies. To investigate the run-in behavior short-term tests were performed whereas steady-state conditions were verified by long-term experiments. The microstructural evolution as well as the tribochemical reactions beneath the surface was investigated by means of cross-sections. The following conclusions can be drawn:

(1) The friction behavior of the tested samples during run-in is dependent on load and initial microstructure which can be traced back to differences in hardness and oxidation kinetics.

(2) The steady state COF is the same for all tested samples ($\mu_{steady} \approx 0.3$) and independent of load or initial microstructure.

(3) During tribological testing three zones can be identified which are a metal/oxide composite zone, a zone showing either grain refinement or coarsening (depending on the initial microstructure) and an unaffected zone (original microstructure).

(4) Regarding the microstructural evolution with increasing sliding cycles in the depth of the wear track, it can be stated that coarse microstructures show a grain refinement whereas finer microstructures undergo grain coarsening. This leads to comparable grain sizes near the surface for all samples irrespective of the initial microstructure. Interestingly, these effects are mainly a result of the large accumulated strain and are not thermally-driven which is in good agreement with results found during severe plastic deformation of nickel.

(5) The formation of sub-surface swirled regions consisting of a metal-oxide composite aids in the stabilization of the microstructure at a steady state mean grain size.

(6) After at most 2,000 sliding cycles all samples show similar contact conditions, topographies and comparable superficial microstructures leading to an almost identical steady-state friction behavior.

The results presented in this manuscript highlight the effectiveness of linking microstructural development at different length scales with the interpretation of macroscopic behaviors (such as friction and wear). Furthermore, the points raised in the discussion could be transferrable to other cubic metals, which under the same type of stress situation, show similar microstructural evolution and deformation mechanisms as the one chosen for this analysis.

Acknowledgements

The authors wish to acknowledge the EFRE Funds of the European Commission for support of activities within the AME- Lab project. S. Suarez acknowledges financial support from the Deutsche Forschungsgemeinschaft (DFG, project ID: SU 911/1-1).

References

[1] Sedlaček M, Podgornik B, Vižintin J. Influence of surface preparation on roughness parameters, friction and wear. *Wear* **266**(3–4): 482–487 (2009)

[2] Meine K, Schneider T, Spaltmann D, Santner E. The influence of roughness on friction Part I: The influence of a single step. *Wear* **253**(7–8): 725–732 (2002)

[3] Mishra R, Basu B, Balasubramaniam R. Effect of grain size on the tribological behavior of nanocrystalline nickel. *Mater Sci Eng A* **373**(1–2): 370–373 (2004)

[4] Argibay N, Chandross M, Cheng S, Michael J R. Linking microstructural evolution and macro-scale friction behavior in metals. *J Mater Sci* **52**(5): 2780–2799 (2017)

[5] Wang L, Gao Y, Xu T, Xue Q. A comparative study on the tribological behavior of nanocrystalline nickel and cobalt coatings correlated with grain size and phase structure. *Mater Chem Phys* **99**(1): 96–103 (2006)

[6] Shafiei M, Alpas A T. Friction and wear mechanisms of nanocrystalline nickel in ambient and inert atmospheres. *Metall Mater Trans A Phys Metall Mater Sci* **38 A**(7): 1621–1631 (2007)

[7] Shafiei M, Alpas A T. Effect of sliding speed on friction and wear behaviour of nanocrystalline nickel tested in an argon atmosphere. *Wear* **265**(3–4): 429–438 (2008)

[8] Singh Raman R K, Khanna A S, Tiwari R K, Gnanamoorthy J B. Influence of grain size on the oxidation resistance of 2 4 1 Cr-1Mo steel. *Oxid Met* **37**(1–2): 1–12 (1992)

[9] Rigney D A. Transfer, mixing and associated chemical and mechanical processes during the sliding of ductile materials. *Wear* **245**(1–2): 1–9 (2000)

[10] Rigney D A, Fu X Y, Hammerberg J E, Holian B L, Falk M L. Examples of structural evolution during sliding and shear of ductile materials. *Scr Mater* **49**(10): 977–983 (2003)

[11] Prasad S V, Battaile C C, Kotula P G. Friction transitions in nanocrystalline nickel. *Scr Mater* **64**(8): 729–732 (2011)

[12] Qi Z, Jiang J, Meletis E I. Wear mechanism of nanocrystalline metals. *J Nanosci Nanotechnol* **9**(7): 4227–4232 (2009)

[13] Cordill M J, Moody N R, Prasad S V., Michael J R, Gerberich W W. Characterization of the mechanical behavior of wear surfaces on single crystal nickel by nanomechanical techniques. *J Mater Res* **24**(3): 844–852 (2009)

[14] Wasekar N P, Haridoss P, Seshadri S K, Sundararajan G. Sliding wear behavior of nanocrystalline nickel coatings: Influence of grain size. *Wear* **296**(1–2): 536–546 (2012)

[15] Prasad S V., Michael J R, Christenson T R. EBSD studies on wear-induced subsurface regions in LIGA nickel. *Scr Mater* **48**(3): 255–260 (2003)

[16] Oleszak D, Shingu P H. Nanocrystalline metals prepared by low energy ball milling. *J Appl Phys* **79**(6): 2975–2980 (1996)

[17] Fecht H J, Hellstern E, Fu Z, Johnson W L. Nanocrystalline metals prepared by high-energy ball milling. *Metall Trans A* **21**(9): 2333–2337 (1990)

[18] Koch C C. Synthesis of nanostructured materials by mechanical milling: problems and opportunities. *Nanostructured Mater* **9**(1–8): 13–22 (1997)

[19] Pippan R, Scheriau S, Taylor A, Hafok M, Hohenwarter A, Bachmaier A. Saturation of fragmentation during severe plastic deformation. *Annu Rev Mater Res* **40**(1): 319–343 (2010)

[20] Mohamed F A, Dheda S S. On the minimum grain size obtainable by high-pressure torsion. *Mater Sci Eng A* **558**: 59–63 (2012)
[21] Williamson G K, Hall W H. X-ray line broadening from filed aluminium and wolfram. *Acta Metall* **1**(1): 22–31 (1953)
[22] Jackson R L, Green I. On the modeling of elastic contact between rough surfaces. *Tribol Trans* **54**(2): 300–314 (2011)
[23] Budynas R G, Nisbett J K. *Shigley's Mechanical Engineering Design*. New York (NY, USA): McGraw-Hill, 2011
[24] Hutchings I, Shipway P. *Tribology: Friction and Wear of Engineering Materials*. Oxford (UK): Butterworth-Heinemann, 2017
[25] Lide D R, ed. *CRC Handbook of Chemistry and Physics*. Boca Raton (FL, USA): CRC Press (Taylor and Francis Group), 2005
[26] Blau P J. On the nature of running-in. *Tribol Int* **38**(11–12 SPEC. ISS.): 1007–1012 (2005)
[27] Chandross M, Curry J F, Babuska T F, Lu P, Furnish T A, Kustas A B, Nation B L, Staats W L, Argibay N. Shear-induced softening of nanocrystalline metal interfaces at cryogenic temperatures. *Scr Mater* **143**: 54–58 (2018)
[28] Sullivan J L, Quinn T F J, Rowson D M. Developments in the oxidational theory of mild wear. *Top Catal* **13**(4): 153–158 (1980)
[29] Zum Gahr K H. *Microstructure and Wear of Materials* (*Tribology Series)*. Amsterdam (NL): Elsevier Science Publishers B.V., 1987
[30] Valiev R Z, Islamgaliev R K, Alexandrov I V. Bulk nanostructured materials from severe plastic deformation. *Prog Mater Sci* **45**(2): 103–189 (2000)
[31] Doherty R D, Hughes D A, Humphreys F J, Jonas J J, Juul Jensen D, Kassner M E, King W E, McNelley T R, McQueen H J, Rollett A D. Current issues in recrystallization: A review. *Mater Sci Eng A* **238**(2): 219–274 (1997)
[32] Heilmann P, Clark W A T, Rigney D A. Orientation determination of subsurface cells generated by sliding. *Acta Metall* **31**(8): 1293–1305 (1983)
[33] Rigney D A. Large strains associated with sliding contact of metals. *Mater Res Innov* **1**: 231–234 (1998)
[34] Bachmaier A, Hohenwarter A, Pippan R. New procedure to generate stable nanocrystallites by severe plastic deformation. *Scr Mater* **61**(11): 1016–1019 (2009)
[35] Yang B, Vehoff H, Hohenwarter A, Hafok M, Pippan R. Strain effects on the coarsening and softening of electro-deposited nanocrystalline Ni subjected to high pressure torsion. *Scr Mater* **58**(9): 790–793 (2008)

Sebastian SUAREZ. He received his Electromechanical Engineering degree in 2008 from the National Technical University in Argentina and his Ph.D. degree in materials science and engineering in 2014 from Saarland University, Germany. He currently leads the Materials Engineering group at the Chair of Functional Materials (Saarland University). His research focuses on the design and implementation of new nanocarbon-based materials for tribological and electrical applications.

Philipp GRÜTZMACHER. He received his B.Eng. degree in materials engineering from the Nuremberg Institute of Technology Georg Simon Ohm, Germany, in 2012 and his M. Sc. degree in advanced materials science and engineering from Saarland University and the Polytechnic University of Catalonia in 2014. Since 2015, he pursues his PhD studies at the Chair of Functional Materials (Saarland University). His current research interests focus on tribology, laser surface texturing, and surface engineering.